Heliyon

ELSEVIER

Received:
16 October 2018
Revised:
10 December 2018
Accepted:
4 February 2019

Cite as: Fazle Mabood, Kalidas Das. Outlining the impact of melting on MHD Casson fluid flow past a stretching sheet in a porous medium with radiation. Heliyon 5 (2019) e01216. doi: 10.1016/j.heliyon.2019.e01216

Outlining the impact of melting on MHD Casson fluid flow past a stretching sheet in a porous medium with radiation

Fazle Mabood [a,*], **Kalidas Das** [b]

[a] *School of Information Technology, Fanshawe College London, ON, Canada*

[b] *Department of Mathematics, Krishnagar Govt. College, Krishnagar, 741101, Nadia, WB, India*

[*] Corresponding author.

E-mail address: mabood1971@yahoo.com (F. Mabood).

Abstract

This article focused on framing the features of melting heat transfer on magnetohydrodynamic (MHD) Casson fluid flow in a porous medium influenced by thermal radiation. The present model is employed to simulate the viscoelastic behavior of fluid in the porous regime. Firstly, the governing partial differential equations are converted into ordinary differential equations via suitable similarity transformation and then solved the developed nonlinear equations by using Runge-Kutta Fehlberg-45 order method. A detailed analysis of certain parameters on the velocity, temperature, skin friction coefficient, and reduced Nusselt number are illustrated and examined. The results indicate that enlargement in M and Ω decline velocity profile but an opposite trend for temperature. Furthermore, an increment in R and Me results in uphill Nusselt number. The results of the present analysis are compared with the available works in particular situations and more agreement has been observed.

Keywords: Computational mathematics, Mechanics, Thermodynamics

https://doi.org/10.1016/j.heliyon.2019.e01216

1. Introduction

In view of specified feature of final products depending mainly upon the rate of heat transfer, the flow and heat transfer mechanism through stretching surfaces find many peer-to-peer applications such as manufacturing of fiber-glass, enhancement in efficiency of paints and lubrication, plastic-molding, glass blowing, paper production, crystal growing, aerodynamic extrusion of polymer and rubber sheets and many others. Crane [1] was the pioneer who analyzed beautifully the flow over a linear stretching plate and obtained successfully the analytical solution for the Navier-Stokes equations.

Later, heat transfer characteristics of Newtonian and non-Newtonian fluids flow were well addressed by various researchers [2, 3, 4, 5]. Majeed et al. [6] prescribed the effect of suction over a stretching surface for ferromagnetic Non-Newtonian fluid flow. Several industrial manufacturing processes involve non-Newtonian fluids such as paints, lubricants, polymeric suspensions, biological fluids, animal blood, colloidal solutions, and liquid crystals with rigid molecules, which cannot be described by traditional Newtonian fluid behaviors. There are many non-Newtonian fluid models available in open literature [7, 8, 9, 10]. One such model is Casson fluid which has distinctive features. Recently, Mahdy [11] presented the effects of variable wall temperature for mixed Casson nanofluid flow for rotating sphere at stagnation point, Mabood et al. [12] analyzed the impact of radiation on a moving surface for Casson fluid in porous medium, Ibrahim et al. [13] addressed the characteristics of heat transmission on dissipative convective Casson nanofluid with chemical reaction, heat source and slip condition.

Magnetohydrodynamic (MHD) is additionally a functioning zone of present day building sciences and includes the communication of magnetic fields and electrically conducting fluids. MHD pipe flows emerge in ionized quickening agents, MHD flow control in atomic reactors, MHD sidestep vitality generators, fluid metal manufacture forms, bubble levitation and so on [14]. Kumar et al. [15] numerically discussed MHD effects for non-Newtonian fluid over a stretching surface in porous regime under the influence of nonlinear radiation, Kumar and co-workers [16, 17] explored various aspects of MHD effects for non-Newtonian fluid such as: Carreau, Williamson, and Micropolar fluids.

The problem of melting heat transfer has accomplished significantly by researchers due to its wider range of technological and industrial based applications in preparation of semiconductor substance thawing of frozen grounds and solidification of molten rock flows etc. Bachok et al. [18] investigated the steady flow over moving surface for the study of melting heat transfer, Yacob et al. [19] analyzed micropolar fluid for melting heat transfer on stagnation point over a stretching/shrinking surfaces. Mabood and Das [20] illustrated the effect of second-order slip and melting

https://doi.org/10.1016/j.heliyon.2019.e01216

heat transfer with radiation for MHD nanofluid flow. Mustafa et al. [21] have been presented the effect of melting heat transfer on stagnation point flow of Jeffrey fluid. For the effect of external of the magnetic field, Das and Zheng [22] have further investigated the work of Mustafa et al. [21].

Heat transfer determined by thermal radiation has vast application in different technological process, including missiles, nuclear power plant, satellites and space vehicles, gas turbines and the generate thrust device for aircraft engine. Makinde [23] studied vertical porous surface for free convection with radiation. Hayat et al. [24] examined MHD mixed convection of stagnation point flow past a vertical stretching sheet with radiation. Das [25] discussed slip and radiation effects on MHD flow over a flat plate. Hayat et al. [26] discussed the thermal radiation characteristics of Jeffrey fluid, Sandeep et al. [27] examined the effects of magnetic nanoparticles in MHD nanofluid flow, Ramadev et al. [28] have presented variable thickness melting on MHD Carreau fluid. More interesting investigations on heat transfer on natural convection, MHD and porous medium can be seen [29, 30, 31, 32, 33, 34, 35, 36, 37, 38, 39, 40].

Literature survey reveals that a lot of work has been done by various researchers to examine the characteristics of heat transfer due to melting in the fluid flows. The phenomenon of melting heat transfer is not investigated up to yet on stretching surface with radiation in porous surface. Hence our main objective is to fill such a gap. The effects of transverse magnetic field and melting effect are included in the presence of thermal radiation. Numerical results for flow equations are obtained and discussion is provided for several values of pertinent parameters governing the problem.

2. Model

We suppose two-dimensional steady flow of a Casson fluid over a horizontal linear stretching sheet in a porous medium of permeability$K$, melting at a steady rate into a constant property as shown in Fig. 1. The fluid is electrically conducting in the presence of a uniform transverse magnetic fieldB_0. The induced magnetic field is negligible. Consider external flow is $u_e(x) = ax$and the velocity of the stretching sheet is$u_w(x) = cx$, where a and and c are positive constant and$x$is the coordinate considered along the stretching sheet. We assumed that both T_m and T_∞ are the melting and free stream temperature of the fluid respectively, where $T_\infty > T_m$. The rheological equation of the Casson fluid is given by:

$$\tau_{ij} = \begin{cases} 2\left(\mu_B + P_y \Big/ \sqrt{2\pi}\right) e_{ij}, & \pi > \pi_c, \\ 2\left(\mu_B + P_y \Big/ \sqrt{2\pi_c}\right) e_{ij}, & \pi > \pi_c, \end{cases} \tag{1}$$

where μ_B plastic dynamic viscosity, $\pi = e_{ij}e_{ij}$ and e_{ij} is the $(i,j)^{th}$ component of deformation rate, π denotes deformation rate, π_c is a critical value of non-

https://doi.org/10.1016/j.heliyon.2019.e01216

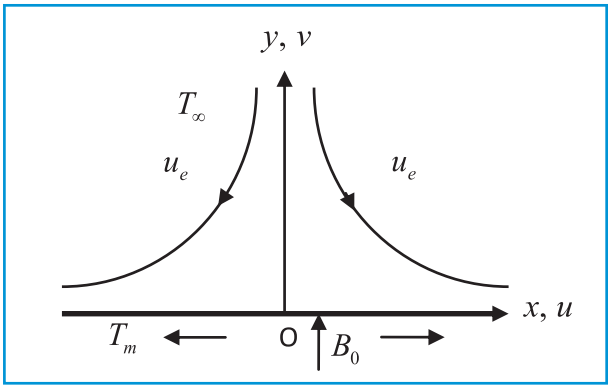

Fig. 1. Physical model and coordinate system.

Newtonian model, P_y is the yield stress of fluid. Under these assumptions, the governing equations are [12, 13]:

$$\frac{\partial u}{\partial x}+\frac{\partial v}{\partial y}=0, \tag{2}$$

$$u\frac{\partial u}{\partial x}+v\frac{\partial u}{\partial y}=u_e\frac{du_e}{dx}+\nu\left(1+\frac{1}{\beta}\right)\frac{\partial^2 u}{\partial y^2}-\frac{\sigma B_0^2}{\rho}(u-u_e)-\frac{\nu}{K}(u-u_e), \tag{3}$$

$$u\frac{\partial T}{\partial x}+v\frac{\partial T}{\partial y}=\alpha\frac{\partial^2 T}{\partial y^2}-\frac{1}{\rho c_p}\frac{\partial q_r}{\partial y}, \tag{4}$$

consider the boundary conditions of Eqs. (1), (2), (3), and (4) are the following

$$\begin{aligned} &u=u_w(x)=cx, \quad T=T_m, \quad \text{at} \quad y=0,\\ &u\to u_e(x)=ax, \quad T\to T_\infty, \quad \text{as} \quad y\to\infty, \end{aligned} \tag{5}$$

and

$$k\left(\frac{\partial T}{\partial y}\right)_{y=0}=\rho[\lambda+c_s(T_m-T_0)]v(x,0), \tag{6}$$

Here α the thermal diffusivity of the fluid, K permeability of the medium, $(u,\ v)=$ velocity components along axes, k thermal conductivity, β Casson fluid parameter, σ electrical conductivity of fluid, λ latent heat of the fluid, ν kinematic viscosity of the fluid, c_s heat capacity of the solid surface, ρ the density of fluid, q_r radiative heat flux and $c_p$the specific heat at constant pressure.

By the use of Rosseland approximation for radiation, we have

$$q_r=-\frac{4\sigma^*}{3k^*}\frac{\partial T^4}{\partial y}, \tag{7}$$

https://doi.org/10.1016/j.heliyon.2019.e01216

where σ^* Stefan−Boltzmann constant, and $k^*$the absorption coefficient and $T^4 \approx 4T_\infty{}^3 T - 3T_\infty{}^4$. Therefore, Eq. (4) turns to:

$$u\frac{\partial T}{\partial x} + \mathrm{v}\frac{\partial T}{\partial y} = \alpha\frac{\partial^2 T}{\partial y^2} + \frac{16\sigma^* T_\infty{}^3}{3\rho c_p k^*}\frac{\partial^2 T}{\partial y^2}, \tag{8}$$

The similarity variables are [14]:

$$\psi = x\sqrt{av} f(\eta), \qquad \theta(\eta) = \frac{T - T_m}{T_\infty - T_m}, \qquad \eta = y\sqrt{\frac{a}{\nu}}, \tag{9}$$

where $\psi$is the stream function defined in such a way that $u = \frac{\partial \psi}{\partial y}andv = -\frac{\partial \psi}{\partial x}$ which automatically satisfies the continuity Eq. (1). By using this definition, we obtain:

$$u = a\,x f'(\eta), \qquad v = -\sqrt{a\,\nu} f(\eta), \tag{10}$$

substitute Eqs. (9) and (10) into Eqs. (3) and (8), the transformed equations are:

$$\left(1 + \frac{1}{\beta}\right) f''' + f f'' - f'^2 + (M + \Omega)(1 - f') + 1 = 0, \tag{11}$$

$$(1 + R)\theta'' + \mathrm{Pr} f\theta' = 0. \tag{12}$$

The corresponding boundary conditions:

$$f'(0) = \varepsilon,\ \mathrm{Pr} f(0) + Me\theta'(0) = 0,\ \theta(0) = 0,\ f'(\infty) = 1,\ \theta(\infty) = 1, \tag{13}$$

where the primes denote differentiation with respect to η, $\beta = \mu_B\sqrt{2\pi_c}/P_y$ non-Newtonian Casson fluid parameter, $M = \sigma B_0^2/\rho\, a$ magnetic parameter, $\Omega = \nu/K\, a$ permeability parameter, $R = 16\sigma^* T_\infty^3/3k^* k$ radiation parameter, $\varepsilon = c/a$ stretching parameter, $\mathrm{Pr} = \nu/\alpha$ Prandtl number, $Me = \frac{c_p(T_\infty - T_m)}{\lambda + c_s(T_m - T_0)}$ melting parameter and Me combination of the Stefan numbers $c_p(T_\infty - T_m)/\lambda$ and $c_s(T_m - T_0)/\lambda$ for the liquid and solid phases, respectively.

The physical quantities are the skin friction coefficient C_f and the local Nusselt numberNu_x are:

$$C_f = \frac{\tau_w}{\rho u_e^2}\ ,\quad Nu_x = \frac{x q_w}{k(T_\infty - T_m)}, \tag{14}$$

where $\tau_w = \left(1 + \frac{1}{\beta}\right)\left(\frac{\partial u}{\partial y}\right)_{y=0}$ surface shear stress, μ dynamic viscosity of fluid, and $q_w = -k\left(\frac{\partial T}{\partial y}\right)_{y=0} + q_r$surface heat flux.

Using Eq. (9), the skin friction coefficient is:

https://doi.org/10.1016/j.heliyon.2019.e01216

$$C_f = \frac{\tau_w}{\rho u_e^2} \quad \Rightarrow \quad \mathrm{Re}_x^{1/2} C_f = \left(1 + \frac{1}{\beta}\right) f''(0), \tag{15}$$

and the Nusselt number is:

$$Nu_x = \frac{x q_w}{k(T_\infty - T_m)} \quad \Rightarrow \quad \mathrm{Re}_x^{-1/2} Nu_x = -(1+R)\theta'(0), \tag{16}$$

where $\mathrm{Re}_x = u_e x/\nu$represent the local Reynolds number.

It is interesting to note that when $M = \Omega = R = 0, \ \beta \to \infty$ in Eqs. (11) and (12), our model reduces to those reported by Bachok et al. [18].

3. Methodology

Results obtained by means of Runge-Kutta Fehlberg fourth fifth method are endorsing that the tool is well-matched, efficient, accurate, appropriate and reliable to examine the solutions of nonlinear problems. The method of solution as described in [41] are provided step wise:

$$k_0 = f(x_i, \ y_i),$$

$$k_1 = f\left(x_i + \frac{1}{4}h, \ y_i + \frac{1}{4}hk_0\right),$$

$$k_2 = f\left(x_i + \frac{3}{8}h, \ y_i + \left(\frac{3}{32}k_0 + \frac{9}{32}k_1\right)h\right),$$

$$k_3 = f\left(x_i + \frac{12}{13}h, \ y_i + \left(\frac{1932}{2197}k_0 - \frac{7200}{2197}k_1 + \frac{7296}{2197}k_2\right)h\right),$$

$$k_4 = f\left(x_i + h, \ y_i + \left(\frac{439}{216}k_0 - 8k_1 + \frac{3860}{513}k_2 - \frac{845}{4104}k_3\right)h\right),$$

$$k_5 = f\left(x_i + \frac{1}{2}h, \ y_i + \left(-\frac{8}{27}k_0 + 2k_1 - \frac{3544}{2565}k_2 + \frac{1859}{4104}k_3 - \frac{11}{40}k_4\right)h\right),$$

$$y_{i+1} = y_i + \left(\frac{25}{216}k_0 + \frac{1408}{2565}k_2 + \frac{2197}{4104}k_3 - \frac{1}{5}k_4\right)h,$$

$$z_{i+1} = z_i + \left(\frac{16}{135}k_0 + \frac{6656}{12825}k_2 + \frac{28561}{56430}k_3 - \frac{9}{50}k_4 + \frac{2}{55}k_5\right)h, \tag{17}$$

where y is the fourth-order Runge-Kutta and z is the fifth- order Runge-Kutta. An estimate of the error can be obtained by subtracting the two values obtained. If the error exceeds a specific threshold, the results can be recalculated using a smaller step size. The approach to estimating the new step size is given below:

https://doi.org/10.1016/j.heliyon.2019.e01216

Table 1. Comparison of $f''(0)$ and $-\theta'(0)$ for different values of ε and Me when $\Pr = 1,\ M = \Omega = R = 0$, and $\beta \to \infty$.

Parameters		Yacob et al. [19]		Present results	
ε	Me	$f''(0)$	$-\theta'(0)$	$f''(0)$	$-\theta'(0)$
0.0	0	1.232588	-0.570465	1.232588	-0.570465
	1	1.037003	-0.361961	1.037003	-0.361961
0.5	0	0.713295	-0.692064	0.713295	-0.692064
	1	0.599090	-0.438971	0.599090	-0.438971
2.0	0	-1.887307	-0.979271	-1.887307	-0.979271
	1	-1.580483	-0.621187	-1.580484	-0.621187
5.0	0	-10.264749	-1.396355	-10.264749	-1.396355
	1	-7.195937	-0.886425	-8.5746752	-0.886425
6.0	0	-	-	-13.774813	-1.511165
	1	-	-	-11.501531	-0.959514

$$h_{new} = h_{old}\left(\frac{\varepsilon h_{old}}{2|z_{i+1} - y_{i+1}|}\right)^{1/4}. \tag{18}$$

We assume$\Delta\eta = 0.01$, the criterion convergence is less than 10^{-6}, and value for $\eta_{\max} = 8$:

In Tables 1, 2, and 3, the accuracy of the present method can be verified by comparing with the previous results of Bachok et al. [18] and Yacob et al. [19] for $M = \Omega = R = 0$, $\Pr = 1$ or 7, and $\beta \to \infty$ where it is observed that there is a good agreement between them. The good agreement is related to the observation that increases in melting parameter decline the skin friction coefficient significantly.

Table 2. Comparison of $f''(0)$ for different values of ε and Me when $\Pr = 1,\ M = \Omega = R = 0$, and $\beta \to \infty$.

ε	Bachok et al. [18]				Present results			
	$Me = 0$	$Me = 1$	$Me = 2$	$Me = 3$	$Me = 0$	$Me = 1$	$Me = 2$	$Me = 3$
0.0	1.232588	1.037003	0.946851	0.891381	1.232588	1.037003	0.946851	0.891381
0.1	1.146561	0.964252	0.880442	0.828948	1.146561	0.964252	0.880442	0.828948
0.2	1.051130	0.883675	0.806876	0.759752	1.051130	0.883675	0.806876	0.759752
0.5	0.713295	0.599089	0.504333	0.515172	0.713295	0.599089	0.547021	0.515172
1.0	0	0	0	0	0	0	0	0
2.0	−1.887307	−1.580484	−1.442747	−1.359211	−1.887307	−1.580484	−1.442747	−1.359211
3.0	-	-	-	-	-4.2765414	-3.577332	-3.265006	-3.076102

https://doi.org/10.1016/j.heliyon.2019.e01216

Table 3. Comparison of $-\theta'(0)$ for different values of Pr and Me when $M = \Omega = R = 0$, and $\beta \to \infty$.

Parameters		Bachok et al. [18]	Present results
Pr	*Me*	$-\theta'(0)$	$-\theta'(0)$
1	0	-0.7978846	- 0.7978846
	1	−0.5060545	−0.5060545
	2	−0.3826383	−0.3826383
	3	−0.3119564	−0.3119564
7	0	−2.1110042	−2.1110041
	1	−1.3388943	−1.3388943
	2	−1.0123657	−1.0123657
	3	−0.8253591	−0.8253591

4. Results & discussion

A comprehensive numerical study is conducted for various physical parameters and results are presented in terms of graphs and tables. Numerical computations are carried out for the stretching parameter $\varepsilon = 0.5$ or 1.5 while magnetic field parameter M, permeability parameter Ω, melting parameter Me, radiation parameter R, non-Newtonian Casson fluid parameter βetc. are varied over a range which is listed in the figure legends.

Fig. 2 shows the variation of velocity profiles withε, M and Ω. It is evident from the plot 2a that the flow rate slows down and reduction in velocity as M increases. This is due to the fact that the Lorentz force has the property to slow down the motion of the conducting fluid in the boundary layer. The similar effect is observed for Ω as shown in Fig. 2b. It is worth mentioning that all of these results occur for $\varepsilon = 1.5$

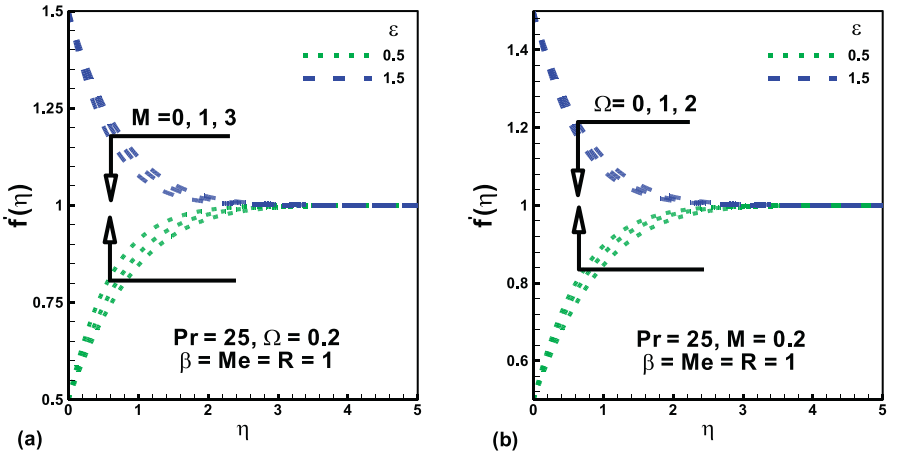

Fig. 2. (a) Effects of M and ε (b) Effects of Ω, ε on the dimensionless velocity.

https://doi.org/10.1016/j.heliyon.2019.e01216

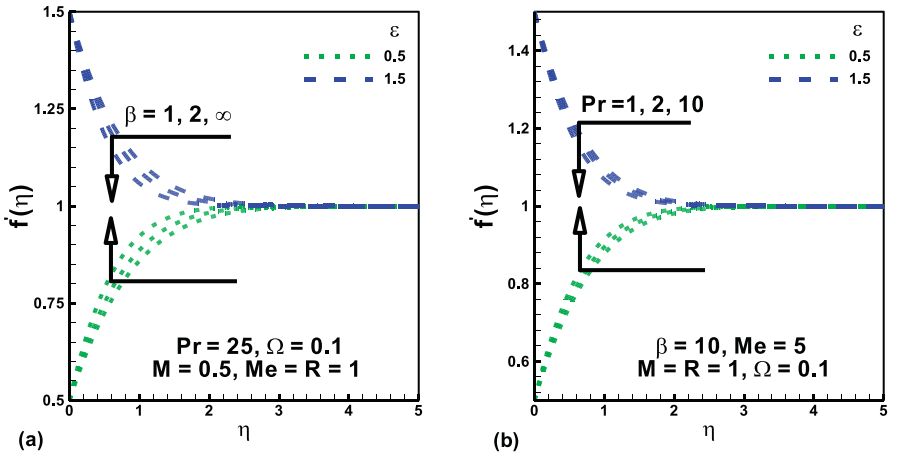

Fig. 3. (a) Effects of β and ε (b) Effects of Pr, ε on the dimensionless velocity.

but the effect is reverse $\varepsilon = 0.5$. The influence of non-Newtonian Casson fluid parameterβ on the velocity is illustrated in Fig. 3. It is noticed that with an increase inβ decrease the magnitude of fluid velocity and so the hydrodynamic boundary layer thickness reduces for higher values ofβ for $\varepsilon = 1.5$ but opposite effect occurs for $\varepsilon = 0.5$. One may note that when βincreases indefinitely, the present phenomena obviously reduce to a Newtonian fluid. Similar results are observed for Prandtl number Pr as depicted in the Fig. 3b. The effect of magnetic parameter M and permeability parameter Ω on the velocity profile of a Casson fluid is accessible in Fig. 4 for lower and higher values ofβ. It is clear from this plot that with increasing values of M and Ω the boundary layer thickness decreases. Further, it is worth noticing from the figure that the effect is prominent for lower values of non-Newtonian Casson fluid parameter β. As an output of these figures, it is understandable that the velocity profile satisfies the asymptotic boundary conditions which support the numerical results obtained.

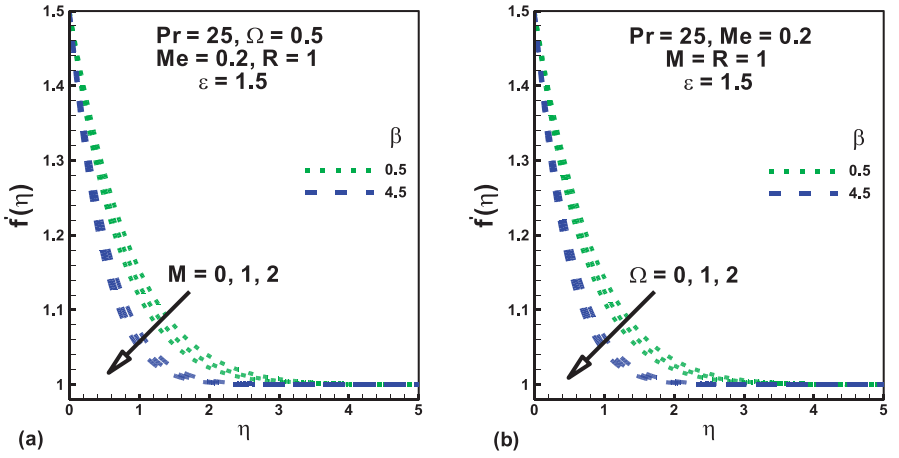

Fig. 4. (a) Effects of M and β (b) Effects of Ω, β on the dimensionless velocity.

https://doi.org/10.1016/j.heliyon.2019.e01216

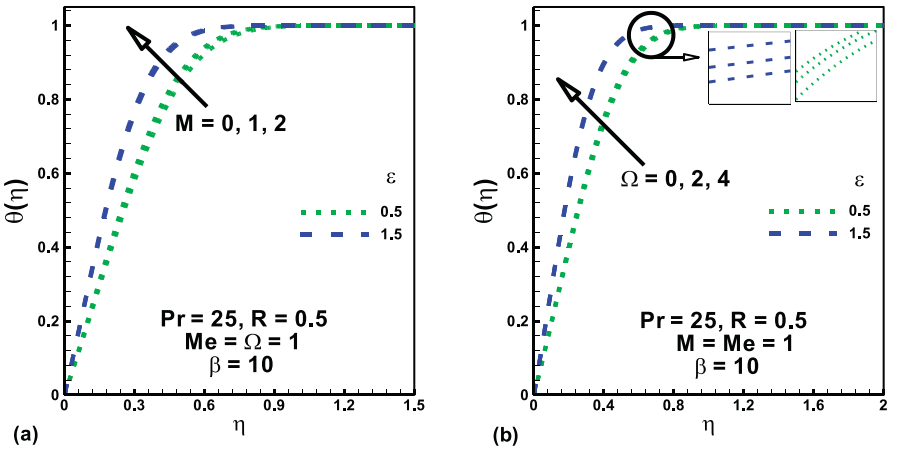

Fig. 5. (a) Effects of M and ε (b) Effects of Ω, ε on the dimensionless temperature.

Fig. 5a depicts the outcome of the magnetic parameter M on temperature over a radiating horizontal stretching sheet for $\varepsilon = 0.5$ or 1.5. It is seen that the temperature enhances due to magnetic parameter M and stretching parameter ε. Further, when $\varepsilon > 0$, the fluid temperature increases with ε in presence of the magnetic field, as displayed in the Fig. 5a. In Fig. 5b, the effect of the permeability parameter Ω over dimensionless temperature profiles is shown graphically. It is observed that an increase of Ω increases the temperature slightly within the region $\eta < 0.8$ (not precisely determined) but outside this region the effect is not significant. Fig. 6a illustrates the effect of Casson fluid parameter βon temperature under the influence of magnetic field. It is peculiar to observe that the thermal boundary layer thickens slightly with the increasing the values of β. But the fluid temperature increases significantly with increasing the values of Pr as presented in the Fig. 6b. Prandtl number represents the ratio between momentum and thermal diffusivities. Higher Prandtl number related to inferior thermal diffusivity. Hence a minor quantity of

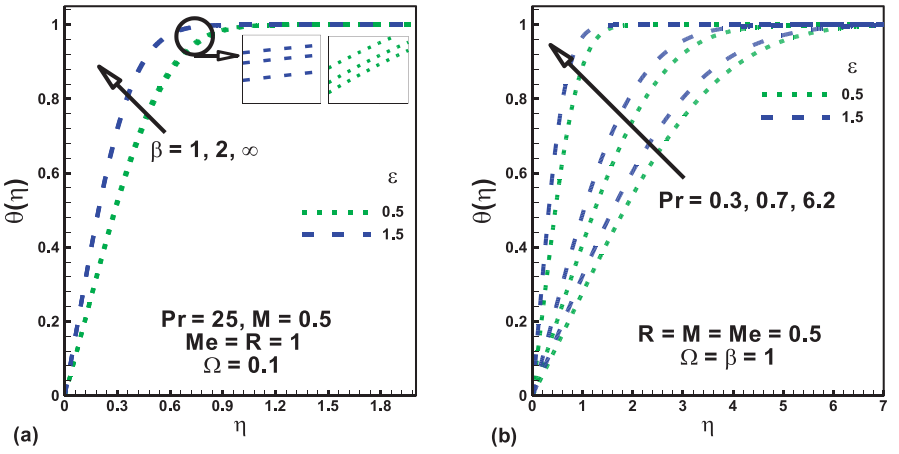

Fig. 6. (a) Effects of β and ε (b) Effects of Pr, ε on the dimensionless temperature.

https://doi.org/10.1016/j.heliyon.2019.e01216

heat is transferred from heated fluid to the melting surface and as a result, the temperature remains higher.

Effect of thermal radiation parameter R on fluid temperature is examined in Fig. 7a for $\varepsilon = 0.5$ or 1.5. It is observed that the temperature retards consistently with increasing thermal radiation parameter. The effect of the melting parameter Me can be seen from the variation of the temperature field $\theta(\eta)$ with the similarity independent variable η as expressed in Fig. 7b. The rise in melting parameter Me the temperature decreases for both values of ε. The reason behind this phenomenon is due to the plunges of a cold sheet into warm water, it starts to melt. As the melting progress, the surface slowly transfers to a liquid state causing the velocity to grow faster, where it causes a decrease in the temperature. As a result, stronger melting leans to increase the thickness of the thermal boundary layer. From these plots, one of the general findings is that the higher values corresponding to the higher temperature.

The variation of the skin friction coefficient$\mathrm{Re}_x^{1/2} C_f$ versus M is displayed in Fig. 8a for different values of non- Newtonian Casson fluid parameter βwhile other parameters are kept fixed. The skin friction coefficient decreases as β increases as shown in Fig. 8a. Fig. 8b depicts the variation of skin friction coefficient with respect to M for different values of permeability parameter Ω and $\varepsilon = 0.5$ or 1.5. From the figure, for any given value of M one may observe that the skin friction coefficient (in the absolute sense) increases with increasing the values of Ω. Further, increasing the values of M causes a rise in the skin friction coefficient at the sheet. The local Nusselt number $\mathrm{Re}_x^{-1/2} Nu_x$ versus M is plotted in Fig. 9a for different values of the non- Newtonian parameterβ while other parameters are kept fixed. It is seen that the local Nusselt number is negative for all values of β which indicate heat flow from the fluid to the solid surface. Further, it is seen from the figure that the heat transfer rate is higher for large values of β. Thus, increasing the non-Newtonian parameterβ

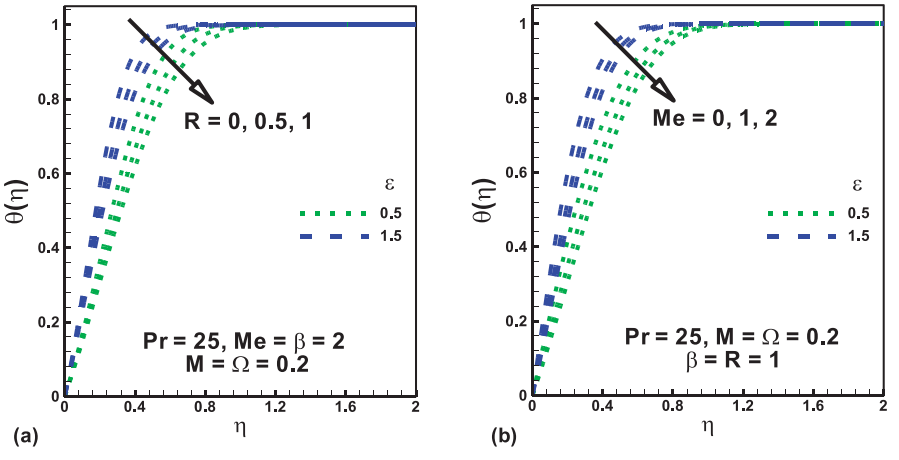

Fig. 7. (a) Effects of R and ε (b) Effects of Me, ε on dimensionless temperature.

https://doi.org/10.1016/j.heliyon.2019.e01216

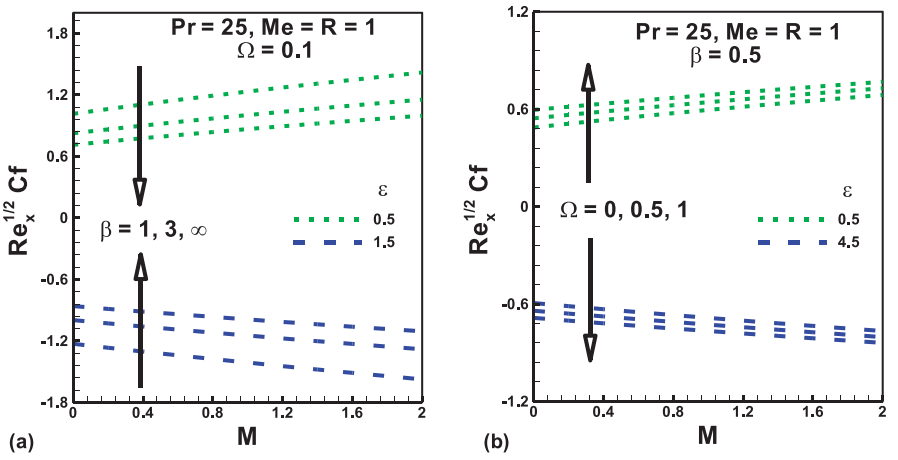

Fig. 8. (a) Effects of M, β and ε (b) Effects of Ω, M and ε on skin friction coefficient.

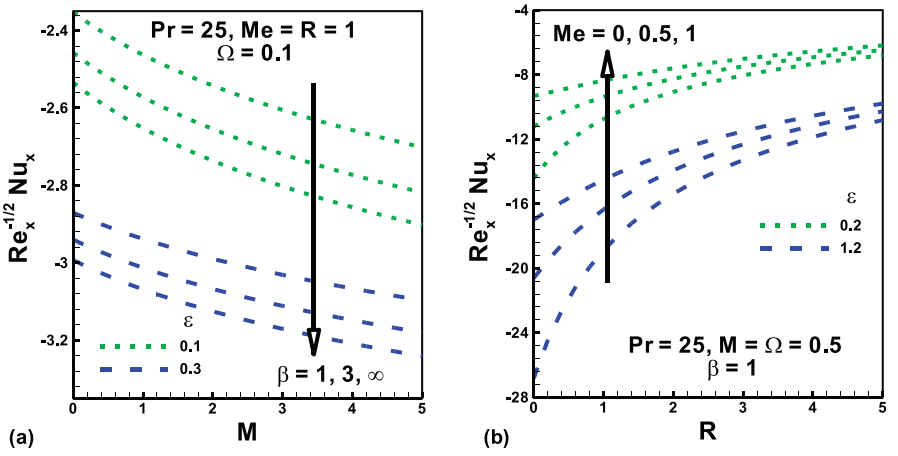

Fig. 9. (a) Effects of M, β and ε (b) Effects of R, Me and ε on heat transfer rate.

increases the Nusselt number at the solid-fluid interface. The influence of melting parameter Me on the Nusselt number is plotted in Fig. 9b with respect to thermal radiation parameter R for $\varepsilon = 0.2$ or 1.2.

The local Nusselt number is reduces with radiation parameter. Further, it is observed with increasing value of melting parameter the absolute value of the temperature gradient at the surface decreases. In addition, it is worth mentioning that the local Nusselt is elevated for large values of ε.

5. Conclusion

The present study gives the numerical solutions for steady boundary layer flow and heat transfer of MHD Casson fluid occurring during the melting process due to a radiating stretching sheet embedded in a porous medium. With the help of similarity transformations, the governing equations are reduced to self-similar non-linear

https://doi.org/10.1016/j.heliyon.2019.e01216

ordinary differential equations which are then solved using Runge−Kutta−Fehlberg method with shooting technique. Main conclusions of the study are as follows:

- ➢ Increasing the magnetic field, permeability parameter and non-Newtonian Casson fluid parameter lead to a deceleration of the fluid velocity which in turn decreases the boundary layer thickness.
- ➢ The fluid temperature and the thermal boundary layer thickness decrease for increasing thermal radiation and melting parameter whereas reverse effect occurs for stretching parameter, permeability parameter, and magnetic field parameter.
- ➢ The skin friction coefficient reduces with an increase in the non-Newtonian parameter whereas the effect is opposite for magnetic and permeability parameters are seen.
- ➢ An increase in the melting and radiation the local Nusselt number at the solid-fluid interface decreases but the opposite effect take place for the Casson fluid parameter.

Declarations

Author contribution statement

Fazle Mabood: Performed the experiments; Contributed reagents, materials, analysis tools or data; Wrote the paper.

Kalidas Das: Conceived and designed the experiments; Analyzed and interpreted the data.

Funding statement

This research did not receive any specific grant from funding agencies in the public, commercial, or not-for-profit sectors.

Competing interest statement

The authors declare no conflict of interest.

Additional information

No additional information is available for this paper.

References

[1] L.J. Crane, Flow past a stretching sheet, J. Appl. Math. Phys. 21 (1970) 645−647.

https://doi.org/10.1016/j.heliyon.2019.e01216

[2] C. Fetecau, R. Ellahi, M. Khan, N.A. Shah, Combine porous and magnetic effects on some fundamental motions of Newtonian fluids over an infinite plate, J. Porous Media 21 (7) (2018) 589−605.

[3] A. Zeeshan, N. Ijaz, T. Abbas, R. Ellahi, The sustainable characteristic of Bio-bi-phase flow of peristaltic transport of MHD Jeffery fluid in human body, Sustainability 10 (8) (2018) 2671.

[4] N. Shehzad, A. Zeeshan, R. Ellahi, Electroosmotic flow of MHD Power law Al2O3-PVC nanofluid in a horizontal channel: Couette-Poiseuille flow model, Commun. Theor. Phys. 69 (6) (2018) 655−666.

[5] A. Majeed, A. Zeeshan, S.A. Alamri, R. Ellahi, Heat transfer analysis in ferromagnetic viscoelastic fluid flow over a stretching sheet with suction, Neural Comput. Appl. 30 (6) (2018) 1947−1955.

[6] A.A. Khan, F. Masood, R. Ellahi, M.M. Bhatti, Mass transport on chemicalized fourth-grade fluid propagating peristaltically through a curved channel with magnetic effects, J. Mol. Liq. 258 (2018) 186−195.

[7] M.M. Bhatti, A. Zeeshan, R. Ellahi, G.C. Shit, Mathematical modeling of heat and mass transfer effects on MHD peristaltic propulsion of two-phase flow through a Darcy-Brinkman-Forchheimer Porous medium, Adv. Powder Technol. 29 (2018) 1189−1197.

[8] R. Ellahi, A. Zeeshan, N. Shehzad, Sultan Z. Alamri, Structural impact of Kerosene-Al2O3 nanoliquid on MHD Poiseuille flow with variable thermal conductivity: application of cooling process, J. Mol. Liq. 264 (2018) 607−615.

[9] S.Z. Alamri, A.A. Khan, A. Zeeshan, R. Ellahi, Effects of mass transfer on MHD second grade fluid towards stretching cylinder: a novel perspective of Cattaneo−Christov heat flux model, Phys. Lett. 383 (2019) 276−281.

[10] F. Mabood, R.G. Abdel-Rahman, G. Lorenzini, Effect of melting heat transfer and thermal radiation on Casson fluid flow in porous medium over moving surface with magnetohydrodynamics, J. Eng. Thermophys. 25 (4) (2016) 536−547.

[11] A. Mahdy, Simultaneous impacts of MHD and variable wall temperature on transient mixed Casson nanofluid flow in the stagnation point of rotating sphere, Appl. Math. Mech. 39 (9) (2018) 1327−1340.

[12] S.M. Ibrahim, P.V. Kumar, G. Lorenzini, E. Lorenzini, F. Mabood, Numerical study of the onset of chemical reaction and heat source on dissipative MHD stagnation point flow of Casson nanofluid over a nonlinear stretching sheet

 https://doi.org/10.1016/j.heliyon.2019.e01216

with velocity slip and convective boundary conditions, J. Eng. Thermophys. 26 (2) (2017) 256–271.

[13] O.A. Bég, S.K. Ghosh, T.A. Bég, Applied Magnetofluid Dynamics: Modelling and Computation, Lambert, Germany, 2011, p. 445.

[14] K.A. Kumar, V. Sugunamma, N. Sandeep, J.V. Ramana Reddy, Numerical examination of MHD nonlinear radiative slip motion of non-Newtonian fluid across a stretching sheet in the presence of porous medium, Heat Transf. Res. (2018).

[15] K.A. Kumar, V. Sugunamma, N. Sandeep, Numerical exploration of MHD radiative Micropolar liquid flow driven by stretching sheet with primary slip: a Comparative Study, J. Non-Equilib. Thermodyn. (2018).

[16] K.A. Kumar, J.V. Ramana Reddy, V. Sugunamma, N. Sandeep, MHD flow of chemically reacting Williamson fluid over a curved/flat surface with variable heat source/sink, Int. J. Fluid Mech. Res. (2019).

[17] K.A. Kumar, B. Ramadevi, V. Sugunamma, Impact of Lorentz force on unsteady bio convective flow of Carreau fluid across a variable thickness sheet with non-fourier heat flux model, Defect Diffusion Forum 387 (2018) 474–497.

[18] N. Bachok, A. Ishak, I. Pop, Melting heat transfer in boundary layer stagnation-point flow towards a stretching/shrinking sheet, Phys. Lett. 374 (2010) 4075–4079.

[19] N.A. Yacob, A. Ishak, I. Pop, Melting heat transfer in boundary layer stagnation-point flow towards a stretching/shrinking sheet in a micropolar fluid, Comput. Fluids 47 (2011) 16–21.

[20] F. Mabood, K. Das, Melting heat transfer on hydromagnetic flow of a nanofluid over a stretching sheet with radiation and second-order slip, Eur. Phys. J. Plus. 3 (2016) 131.

[21] M. Mustafa, T. Hayat, A.A. Hendi, Influence of melting heat transfer in the stagnation-point flow of a Jeffrey fluid in the presence of viscous dissipation, J. Appl. Mech. 79 (2) (2012), 0245011-5.

[22] K. Das, L. Zheng, Melting effects on the stagnation point flow of a Jeffrey fluid in the presence of magnetic field, Heat Transf. Res. 44 (6) (2013) 493–506.

[23] O.D. Makinde, Free convection flow with thermal radiation and mass transfer past a moving vertical porous plate, Int. Commun. Heat Mass Transf. 32 (2005) 1411–1419.

https://doi.org/10.1016/j.heliyon.2019.e01216

[24] T. Hayat, Z. Abbas, I. Pop, S. Asghar, Effects of radiation and magnetic field on the mixed convection stagnation-point flow over a vertical stretching sheet in a porous medium, Int. J. Heat Mass Transf. 53 (2010) 466–474.

[25] K. Das, Impact of thermal radiation on MHD slip flow over a flat plate with variable fluid properties, Heat Mass Transf. 48 (5) (2011) 767–778.

[26] T. Hayat, S.A. Shehzad, A. Alsaedi, Three-dimensional stretched flow of Jeffrey fluid with variable thermal conductivity and thermal radiation, Appl. Math. Mech. 34 (2013) 1481–1494.

[27] N. Sandeep, A.J. Chamkha, I.L. Animasaun, Numerical exploration of magnetohydrodynamic nanofluid flow suspended with magnetite nanoparticles, J. Braz. Soc. Mech. Sci. Eng. 39 (9) (2017) 3635–3644.

[28] B. Ramadev, V. Sugunamma, K.A. Kumar, J.V. Ramana Reddy, MHD flow of Carreau fluid over a variable thickness melting surface subject to Cattaneo-Christov heat flux, Multidis. Mod. Mater. Struct. (2017).

[29] R. Ellahi, S.A. Alamri, A. Basit, A. Majeed, Effects of MHD and slip on heat transfer boundary layer flow over a moving plate based on specific entropy generation, J. Taibah Uni. Sci. 12 (4) (2018) 476–482.

[30] F. Hussain R. Ellahi, A. Zeeshan, Mathematical models of electro magnetohydrodynamic multiphase flows synthesis with nanosized hafnium particles, Appl. Sci. 8 (2018) 275.

[31] M. Hussan, M. Marin, A. Alsharif, R. Ellahi, Convection heat transfer flow of nanofluid in a porous medium over wavy surface, Phys. Lett. 382 (2018) 2749–2753.

[32] A. Purusothaman, N. Nithyadevi, H.F. Oztop, V. Divya, K. Al-Salem, Three dimensional numerical analysis of natural convection cooling with an array of discrete heaters embedded in nanofluid filled enclosure, Adv. Powder Technol. 27 (1) (2016) 268–280.

[33] R. Ellahi, M. Raza, N.S. Akbar, Study of peristaltic flow of nanofluid with entropy generation in a porous medium, J. Porous Media 20 (5) (2017) 461–478.

[34] K.A. Kumar, J.V. Ramana Reddy, V. Sugunamma, N. Sandeep, Magnetohydrodynamic Cattaneo-Christov flow past a cone and a wedge with variable heat source/sink, Alexandria Eng. J. 57 (1) (2016) 435–443.

[35] K.A. Kumar, V. Sugunamma, N. Sandeep, Impact of non-linear radiation on MHD non-aligned stagnation point flow of Micropolar fluid over a convective surface, J. Non-Equilib. Thermodyn. (2018).

 https://doi.org/10.1016/j.heliyon.2019.e01216

[36] N. Sandeep, I.L. Animasaun, Heat transfer in wall jet flow of magnetic-nanofluids with variable magnetic field, Alexandria Eng. J. 56 (2) (2016) 263−269.

[37] A. Purusothaman, D. Venkatachalam, N. Nithyadevi, H.F. Oztop, An analysis on free convection cooling of a 3x3 heater array in rectangular enclosure using Cu-EG-water nanofluid, J. Appl. Fluid Mech. 9 (6) (2016) 3147−3157.

[38] K.A. Kumar, J.V. Ramana Reddy, V. Sugunamma, Impact of cross diffusion on MHD viscoelastic fluid flow past a melting surface with exponential heat source, Multidis. Mod. Mater. Struct. (2017).

[39] S. Shateyi, F. Mabood, MHD mixed convection slip flow near a stagnation-point on a non-linearly vertical stretching sheet in the presence of viscous dissipation, Therm. Sci. 21 (6B) (2017) 2731−2745.

[40] K.A. Kumar, J.V. Ramana Reddy, V. Sugunamma, N. Sandeep, Simultaneous solutions for MHD flow of Williamson fluid over a curved sheet with non-uniform heat source/sink, Heat Transf. Res. (2018).

[41] J.D. Faires, R.L. Burden, Numerical Methods, Cengage Learning, fourth ed., 2012.

https://doi.org/10.1016/j.heliyon.2019.e01216